Novel multi-layer plastic-scintillator-based solid active proton target for inverse-kinematics experiments

Tran, D. T.; Terashima, S.; Ong, H. J.; Hirakawa, K.; Matsuda, Y.; Aoi, N.; Harakeh, M. N.; Itoh, M.; Kawabata, T.; Kohda, A.

Published in:
Nuclear instruments & methods in physics research section a-Accelerators spectrometers detectors and associated equipment

DOI:
10.1016/j.nima.2020.163514

Publication date:
2020

Nuclear Inst. and Methods in Physics Research, A 959 (2020) 163514

Contents lists available at ScienceDirect

Nuclear Inst. and Methods in Physics Research, A

journal homepage: www.elsevier.com/locate/nima

Novel multi-layer plastic-scintillator-based solid active proton target for inverse-kinematics experiments☆

D.T. Tran [a,b], S. Terashima [c], H.J. Ong [a,*,1], K. Hirakawa [a], Y. Matsuda [d], N. Aoi [a], M.N. Harakeh [e,f], M. Itoh [d], T. Kawabata [g], A. Kohda [a], S.Y. Matsumoto [h], T. Nishi [i], J. Okamoto [d], I. Tanihata [a,c]

[a] Research Center for Nuclear Physics (RCNP), Osaka University, Ibaraki, Osaka 567-0047, Japan
[b] Institute of Physics, Vietnam Academy of Science and Technology, Hanoi 10000, Viet Nam
[c] School of Physics and Nuclear Energy Engineering, Beihang University, Beijing 100191, China
[d] Cyclotron and Radioisotope Center (CYRIC), Tohoku University, Sendai, Miyagi 980-8578, Japan
[e] KVI Center for Advanced Radiation Technology, University of Groningen,, 9747 AA Groningen, The Netherlands
[f] GSI Helmholtzzentrum fur Schwerionenforschung GmbH, Planckstrasse 1, 64291 Darmstadt, Germany
[g] Department of Physics, Osaka University, Osaka 560-0043, Japan
[h] Department of Physics, Kyoto University, Kyoto 606-8502, Japan
[i] RIKEN Nishina Center, Saitama 351-0198, Japan

ARTICLE INFO

Keywords:
Multi-layer plastic scintillators
Solid-state active target
Radioactive isotope beam
Inverse kinematics

ABSTRACT

We have constructed and tested a novel plastic-scintillator-based solid-state active proton target for use in nuclear spectroscopic studies with nuclear reactions induced by an ion beam in inverse kinematics. The active target system, named Stack Structure Solid organic Scintillator Active Target (S^4AT), consists of five layers of plastic scintillators, each with a 1-mm thickness. To determine the reaction point in the thickness direction, we exploit the difference in the energy losses due to the beam particle and the charged reaction product(s) in the scintillator material. S^4AT offers the prospect of a relatively thick target while maintaining a good energy resolution. By considering the relative energy loss between different layers, the energy loss contributed by coincident unreacted beam particles can be eliminated. Such a procedure, made possible by the multi-layer structure, is essential to eliminate the contribution from coincident unreacted beam particles, thus enabling its operation at a moderate beam intensity of up to a few Mcps. We evaluated the performance of S^4AT by measuring the elastic proton–proton scattering using a 70-MeV proton beam at Cyclotron and Radioisotope Center (CYRIC), Tohoku University.

1. Introduction

Nuclei far-removed from the beta-stability line, commonly known as radioactive isotopes or unstable nuclei, are currently at the forefront of nuclear physics research. Over the last few decades, extensive experiments using radioactive-isotope (RI) beams have revealed various exotic and fascinating features of nuclear structure and dynamics hitherto unobserved in nuclei on or near the β-stability line. Of particular interest are the formation of neutron-halo structure [1] and evolution of nuclear magic numbers [2–4] in neutron-rich nuclei. While the exact mechanisms for both phenomena have remained unclear, it seems that the tensor interactions may play an important role [5,6]. The observation of possible effects of the tensor interactions in ^{16}O via (p,d) [7] and (p,dp) [8] reactions on ^{16}O at high-momentum transfer have opened up new possibilities to understand the effect of tensor interactions on the structure of atomic nuclei.

The unstable nuclei, with long isotopic chains, provide the ideal platforms for systematic studies using nuclear reactions. The increasing availability of a wide range of highly- or moderately-intense RI beam species, and developments of more complex and sophisticated detector systems such as multi-strip silicon arrays [9,10] and active gaseous target detector systems [11–15] have enhanced the prospect for spectroscopic studies of unstable nuclei with nuclear reactions. One of the most versatile experimental methods via nuclear reactions is the missing-mass spectroscopy. In this method, the momentum of the reaction product, usually a light ion, is measured. The four-momentum obtained is then used to reconstruct the excitation energy of the residual nucleus right after the reaction, and to determine physical observables such as differential cross sections. To ensure sufficient

☆ The Super-FRS Collaboration.

* Corresponding author.
E-mail address: onghjin@impcas.ac.cn (H.J. Ong).

[1] Present address: Institute of Modern Physics, Chinese Academy of Sciences, Lanzhou, 730000, China.

https://doi.org/10.1016/j.nima.2020.163514
Received 14 November 2019; Received in revised form 10 January 2020; Accepted 21 January 2020
Available online 28 January 2020
0168-9002/

measurement resolution for separating the ground and different excited states in the residual nucleus, it is important to attain good momentum resolution. For experiments with stable beams and stable target nuclei, good momentum resolution is usually fulfilled by using a thin target. The same prescription, however, is seldom applicable to experiments with RI beams due to their limited beam intensities. Hence, to increase luminosity and thereby improve the experimental feasibility, it is essential to increase the target thickness whenever possible. The use of a thicker target, however, may result in the degradation of the momentum resolution due to the uncertainty in the depth of reaction vertex.

Here, we report on the development of a novel multi-layer solid-state active proton target, named Stack Structure Solid organic Scintillator Active Target (S^4AT). The device consists of ordinary commercial plastic scintillators, and is therefore highly affordable and flexible; such advantages have already been demonstrated by the recently developed S^4 neutron detector [16]. S^4AT offers a versatile alternative proton (or deuteron) target for spectroscopic studies with radioactive isotope (RI) beams using nuclear reactions, especially reactions that result in more than one charged particle being ejected, in inverse kinematics. Because the total energy loss of charged particles in the scintillator material differs significantly before and after such reactions, one can determine the reaction point in the thickness direction by measuring the energy-loss distribution across different layers of the active target. This reaction-depth determination capability allows the use of a relatively thick target while maintaining a relatively good energy resolution. The multi-layer structure is of importance because it provides a means to subtract the energy loss due to unreacted beam particles through consideration of the energy-loss difference between adjacent layers. Such feature is essential to eliminate the effect of accompanying unreacted beam (pile-up) particles. These depth-sensitive and pile-up elimination capabilities, together with the short decay time of the plastic scintillator, enable its operation at a moderate beam intensity of up to a few Mcps. To assess the performance of S^4AT, we have conducted a test experiment using elastic proton scattering with a 70-MeV proton beam at Cyclotron and Radioisotope Center (CYRIC), Tohoku University.

The article is organized as follows. In Section 2, we describe the basic principle for vertex determination and the prototype system. The test experiment is presented in Section 3. The data analysis and results are presented in Section 4. Finally, a summary and the future prospects are given in Section 5.

2. Principle for vertex determination and prototype

The present S^4AT prototype was designed to achieve a depth resolution below 0.29 mm (one sigma), or $1/\sqrt{12}$ mm, for the reaction vertex. This depth resolution is necessary to meet our requirement for excitation energy resolutions of about 1 MeV in p(^{6}He,d) and p(^{6}Li,d) reaction measurements in inverse kinematics using 400–800 MeV/u secondary beams at GSI Helmholtzzentrum für Schwerionenforschung GmbH, Darmstadt. The goal of the experiment is to observe possible different effects of tensor interactions in the ground states of ^{6}He and ^{6}Li [17]. In this section, we describe the principle for vertex determination and the constructed prototype.

2.1. Principle for vertex determination

The left diagram of Fig. 1 shows a conceptual drawing of a three-layer plastic-scintillator active-target system. Here, we consider two identical charged beam particles, denoted by A and B, with the same kinetic energy. The particle A reacts with the detector-target nucleus to produce two charged particles C and D. The particle B, on the other hand, traverses the material medium without undergoing any nuclear reaction, losing its energy very gradually in the three plastic scintillators. In the A-induced reactions, however, the measured energy losses in the three layers are very different; the energy loss increases sharply in the second and third layers as compared to the case for the particle B. Hence, by measuring the energy loss in each of the three layers, and considering the energy-loss distribution across the layers, we can determine the reaction point in the thickness direction.

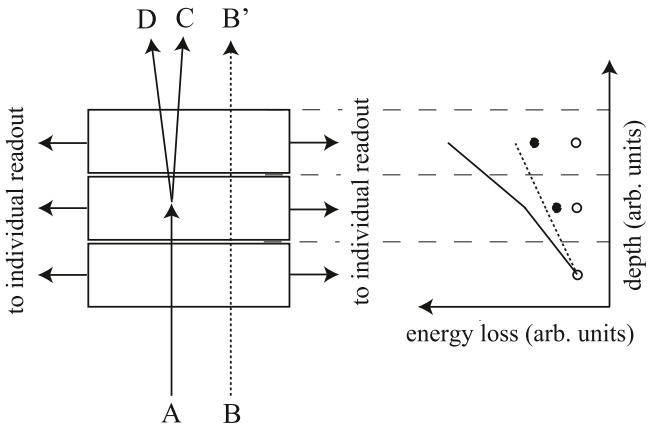

Fig. 1. Conceptual drawing of a three-layer plastic-scintillator active-target system. A and B represent two identical charged beam particles with the same kinetic energy. Whereas A reacts with the detector-target nucleus to produce charged particles C and D, B traverses the material medium without undergoing any nuclear reaction, losing its energy very gradually in the three plastic scintillators. For the A-induced event, however, the measured energy losses in the three layers are very different; the energy loss increases sharply in the second and third layers as compared to the case for the particle B. Right graph shows the energy loss (symbols) and cumulative energy loss (lines) of charged particles in an experiment with a ^{6}He beam. The filled (open) symbol and solid (dotted) line correspond to the A (B)-induced event. See text for details.

The present active target can be used in experiments with nuclear reactions in both normal and inverse kinematics, although its usefulness in the former may be limited. Some examples of the A-induced reactions in normal kinematics are elastic proton–proton ^{1}H(p,p) and proton-deuteron ^{2}H(p,p) scatterings. For reactions in inverse kinematics, a beam of the nucleus of interest, usually with a kinetic energy of the order of several tens of MeV to several GeV, bombards a target. The A-induced reaction then represents reactions in which a beam-like and a target-like particles emerge from the target. Possible reactions include elastic and inelastic scatterings from a proton or deuteron target, transfer reactions such as (p,d), (d,p), (d,t) and (d, ^{3}He), charge-exchange reactions such as (p,n) and (d,2p), proton knockout reactions and multi-nucleon transfer reactions.

To demonstrate the working principle of S^4AT, we consider the p(^{6}He,d) reaction induced by a 400-MeV/u ^{6}He beam, and a layer thickness of 1 mm for S^4AT. In this reaction, the incident ^{6}He beam particle (particle A) is stripped of a neutron by a target proton in S^4AT, leaving the residual ion ^{5}He (particle C) in its ground or excited state. The neutron and the proton stick together to form a deuteron (particle D). Since ^{5}He is particle unbound, it decays almost immediately into a neutron and an α particle. Compared to charged particles, neutrons interact very weakly with matter via the electromagnetic interactions, and thus the measured energy loss in S^4AT is mainly contributed by the deuteron and α. For simplicity, we consider reaction kinematics where both deuteron and α move in the beam direction. Assuming that the reaction occurs at the center of the second layer, the energy of ^{6}He right before the reaction, and those of deuteron and α right after the reaction are 399.7 MeV/u, 31.7 MeV/u and 476.7 MeV/u, respectively. The energy loss by the charged particles in each layer of the plastic scintillators and the cumulative energy loss are shown by the filled symbols and solid line on the right graph of Fig. 1, respectively. The open symbols and dotted line represent the distributions for the non-reacted (B) event. As will be shown in Section 4, for single-hit events, the total energy loss (or even the energy loss in individual layers if the energy resolution is sufficiently good) has a one-to-one correspondence with the depth of reaction. The layer thickness of 1 mm was decided

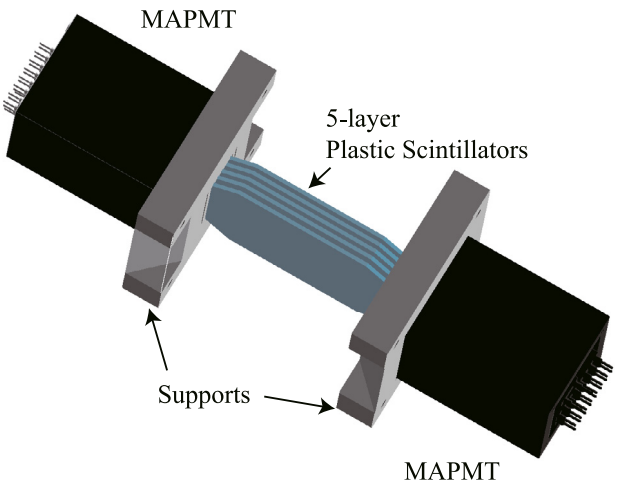

Fig. 2. Schematic drawing of the S^{4}AT prototype.

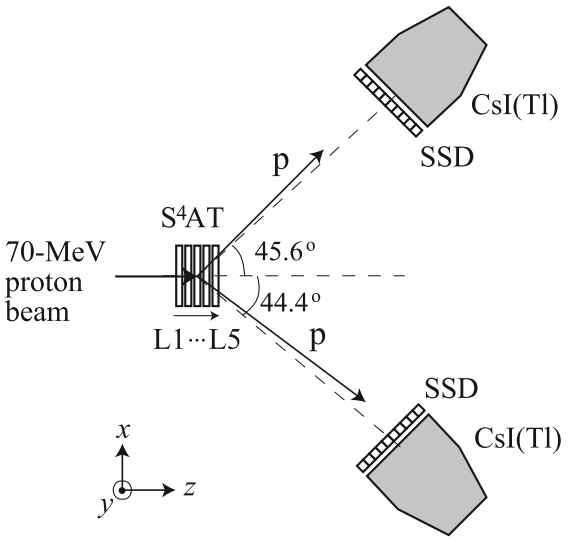

Fig. 3. Schematic layout of the experimental setup. The scale factor is arbitrary; the size of S^{4}AT and the thickness of silicon-strip detectors have been exaggeratedly enlarged for clarity.

based on a simple evaluation using a Monte Carlo simulation, and after taking into account the energy losses and the energy resolution of the plastic scintillators.

The one-to-one correspondence between energy loss and reaction depth may become obscure in the presence of multi-hit events. The probability for multi-hit events increases with increasing beam intensity. The admixture of the B-like particles in the reaction channel of interest will alter the energy-loss distributions, and may in some cases, degrade the energy resolution and undermine its performance as an active target. Such an effect of non-reacted particle(s) can be eliminated by considering the energy-loss difference between adjacent layers. The depth information is reflected in the correlation between energy-loss differences of two pairs of adjacent-layer combinations. This method will be discussed in Section 4.3.

2.2. S^{4}AT prototype

We have constructed a prototype S^{4}AT system. Fig. 2 shows a schematic drawing of the S^{4}AT prototype. The prototype consists of five 1-mm-thick NE-102E-equivalent plastic scintillators, each with a sensitive area of 50 (width) × 30 (height) mm^2. For better light collection and to avoid light leakage, each plastic scintillator is wrapped with a 9-μm-thick aluminized Mylar foil; the foil covers four surfaces which include the two large-area surfaces of the scintillator. The unwrapped sides of the scintillators are connected to two 16-channel Linear Array Multi-Anode Photomultiplier Tube (MAPMT) assemblies H10515B-20 from Hamamatsu Photonics, with which the light outputs are read out. Each anode has a 0.8 × 16 mm^2 sensitive area, and the pitch size of the anodes is 1.0 mm. To prevent light leakage from neighboring scintillators, the plastic scintillators are arranged in parallel at intervals of 1 mm. An opaque support made of Monomer-Cast (MC) Nylon with rectangular holes, also at intervals of 1 mm and sufficient to allow the plastic scintillators through, was mounted before the photocathode on each side of the scintillators to fix their positions.

3. Experiment

The constructed S^{4}AT prototype was tested using elastic proton scattering induced by a 70-MeV proton beam at the 41st beam line of CYRIC, Tohoku University. This reaction was selected because of the similarity between the energy losses of the proton beam and the scattered protons with those of the charged particles in the p(^{6}He,d) reaction with a 400-MeV/u ^{6}He beam, as well as the relatively large cross section and high luminosity. Fig. 3 shows a schematic layout of the experimental setup. The S^{4}AT system was mounted on a target ladder with the 50 × 30-mm^2 surface perpendicular to the beam, and placed at the center of a scattering chamber. We define the axis along the beam direction as the z axis; the x axis is defined as shown in Fig. 3, while the y axis is the axis emerging perpendicularly from the plane of the paper. The S^{4}AT layers from upstream to downstream are denoted as L1–L5 according to their orders in the beam direction. For convenience, we ignore the gap between layers, and define the upstream surface of L1 and the downstream surface of L5 as z=0 and 5 mm, respectively. In addition to S^{4}AT, we also mounted a 170-μm-thick polyethylene (CH_2) target on the target ladder, and used it several times during the experiment to monitor the stability of the beam-energy spread and detector resolution.

To evaluate the depth resolution of S^{4}AT and to enable selection of the elastic scattering channel, we placed two sets of Si-CsI(Tl) telescopes at around 45° with respect to the incident proton beam. The Si-CsI(Tl) telescope with an active area of 50 × 50 mm^2 consists of a 300-μm-thick single-sided silicon-strip detector (SSD) with 10 strips from Hamamatsu Photonics and a 55-mm-thick thallium-doped cesium iodide scintillation crystal from Institute of Modern Physics, Chinese Academy of Sciences. The distance from the target position to the SSDs was about 30 cm. The proton scattering angles were determined from their hit positions on the SSDs, while the kinetic energies were determined from the energy losses in SSDs and CsI(Tl) detectors. The angle subtended by one strip of the SSD, with a 5-mm width, is about 1°. The rear part of the CsI(Tl) crystal (with a thickness of 30 mm) is cut into a trapezoid shape with a reduced area of 30 mm × 30 mm, and is attached to a Si-PIN photodiode S3584-08 from Hamamatsu Photonics. The charge signals from the SSDs and Si-PIN photodiodes were collected and processed by 16-channel charge-sensitive preamplifiers MPR-16 (from Mesytec GmbH & Co) and KPA-16 (from Kaizuworks), respectively. The output signals were later processed by Mesytec's MSCF-16 shaping amplifiers before being fed to 32-channel peak-sensing analog-to-digital converters (MADC-32).

For S^{4}AT, the output signals from MAPMT were sent to a photomultiplier amplifier. One of the two outputs from each channel was sent through a cable delay before being fed into a 32-channel charge-to-digital converter (CAEN V792) module; the other output was fed into a leading-edge discriminator to generate a timing signal, which was mainly used to determine the beam intensity.

Measurements were performed using proton beams with intensities ranging from about 75 kcps to 3.6 Mcps. The beam intensities were

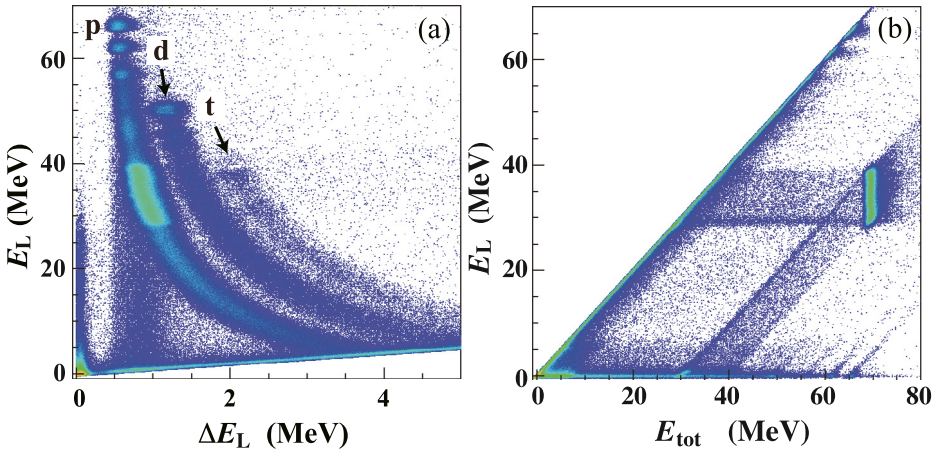

Fig. 4. Energy loss (ΔE) and total energy loss (E) of charged particles in the SSD and SSD-CsI(Tl) detectors during the measurement with the CH_2 target. (a) A scatter plot showing the correlation between the measured E_L and ΔE_L in the left Si-CsI(Tl) telescope. (b) Correlation between the total energy loss measured by the left telescope (E_L) and the summed energy loss in the left and right telescopes ($E_{tot} \equiv E_L + E_R$). The dense locus corresponds to the proton–proton elastic scattering events.

determined combining the scaler information for S^4AT and the telescopes, as well as the relative event numbers from measurements with different beam intensities. For the measurements with the CH_2 target, a beam intensity of about 0.8 nA (about 5000 Mcps) was used. Data acquisition was performed with the logic OR signal of the SSD signals as trigger using the software package babirlDAQ [18].

4. Data analysis and results

The data analyses were performed using the object-oriented data analysis framework, ROOT [19]. Fig. 4(a) shows the correlation between the energy loss (ΔE_L) and total energy loss (E_L) of charged particles in the left SSD and the left SSD-CsI(Tl) telescope for the measurement with the CH_2 target. Three loci corresponding to protons, deuterons and tritons are observed. These particles originated from elastic and inelastic proton scatterings on proton (the dense elongated locus) and ^{12}C, and (p,d) and (p,t) reactions on ^{12}C, respectively. The small clusters distributed along the proton and deuteron loci correspond to the ground and excited states in ^{12}C and ^{11}C. These states, together with the proton–proton elastic scattering events measured at different angles, were used for the energy calibration of the SSD and CsI(Tl) detectors. Fig. 4(b) shows the correlation between the total energy losses measured by the left telescope (E_L) and the summed energy loss in the left and right telescopes ($E_{tot} \equiv E_L + E_R$). The dense locus corresponds to proton–proton elastic scattering events.

The energy resolution of the telescopes for proton scattering was evaluated using the observed discrete states in ^{12}C as well as the proton elastic scattering events during the measurement with the CH_2 target. Since the energy resolutions of the SSDs were below 0.2% for 1-MeV energy loss of protons, and the elastically-scattered protons only deposited less than 5% of their energies in the SSDs compared to the CsI(Tl), we considered only the resolutions of the CsI(Tl) detectors. The widths of the observed discrete states can be attributed to the beam-energy spread, the effect of the target thickness, which includes reaction depth dependence and energy straggling, energy spread due to the reaction kinematics, and the energy resolutions of the CsI(Tl) detectors. To understand the detector response, we performed Monte Carlo simulations with the GEANT4 version 10.03.p01 [20] using the FTFP_BERT physics list. We took into account the experimental setup, which includes the S^4AT detectors and their supports, SSD and CsI(Tl) detectors, as well as the reaction kinematics, beam-energy spread and intrinsic energy resolutions of the detectors. The energy spread due to the target thickness contributes only about 7% (in terms of squared relative uncertainty) to the observed width, and is thus negligible. From comparison between the simulations and the experimental data, the beam-energy spread was found to be less than 200 keV (one sigma). The relative energy resolutions of the CsI(Tl) detectors thus determined consist of three terms [21], namely the stochastic, electronic-noise and constant terms as shown below:

$$\frac{\sigma(E)}{E} = \frac{k_{\text{stochastic}}}{\sqrt{E}} + \frac{k_{\text{electronic}}}{E} + k_{\text{constant}}. \quad (1)$$

$k_{\text{stochastic}}$, $k_{\text{electronic}}$ and k_{constant} are the coefficients with typical values of -0.61 MeV$^{1/2}$, $+2.55$ MeV and $+0.04$, respectively, assuming a 200-keV beam-energy spread. This relation was later used in the simulations for the measurements with S^4AT.

Fig. 5(a) shows similar E_L-ΔE_L plot but for the measurement with S^4AT using a 75-kcps proton beam. The red polygon indicates the typical gate used to select elastically-scattered protons. A similar gate was also defined for the right SSD-CsI(Tl) telescope, and the combined gates were taken as the 'pp-elastic' proton gates. Fig. 5(b) shows the E_L versus E_{tot} plot for the measurement with S^4AT after applying the 'pp-elastic' proton gates. The E_L-E_{tot} plot data are more widely distributed compared to the case for the CH_2 target. The black arrow indicates roughly the depth position of the reaction vertex in the beam direction (L1–L5). The vertical dashed lines in the figure indicate the positions of z=0 and 5 mm, and are only a guide for the eye. The inclined solid line is the equal-energy line which represents the elastically-scattered protons with the same scattering angle. Protons with larger (smaller) scattering angles are distributed below (above) the equal-energy line. The energy spread is larger for reactions in L1 than in L5, and for larger scattering angles than for smaller scattering angles, because the scattered protons had to penetrate more material before reaching the telescopes, and therefore are subjected to more energy-loss straggling and multiple Coulomb scattering.

To determine the depth of the reaction vertex, we apply three methods using the following information: (i) the total energy loss of the scattered protons in the telescopes, (ii) the total energy loss of charged particles in S^4AT, and (iii) energy-loss differences between different layers of S^4AT.

4.1. Vertex determination with SSD-CsI(Tl) telescope

The depth of the reaction vertex was first determined using the summed kinetic energy of the pp-elastic protons measured by the two SSD-CsI(Tl) telescopes. For a reaction at a depth position z_r, the total kinetic energy (denoted by $E_{tot}(z = z_r)$) of the scattered protons (denoted by p_L and p_R) right after the reaction is equal to the kinetic energy of the proton beam right before the reaction $E_B(z_r)$. $E_B(z_r)$ is uniquely determined if we assume a parallel proton beam. The kinetic energies of p_L [$E_L(z_r;\theta_L, z = z_r)$] and p_R [$E_R(z_r;\theta_R, z = z_r)$] depend

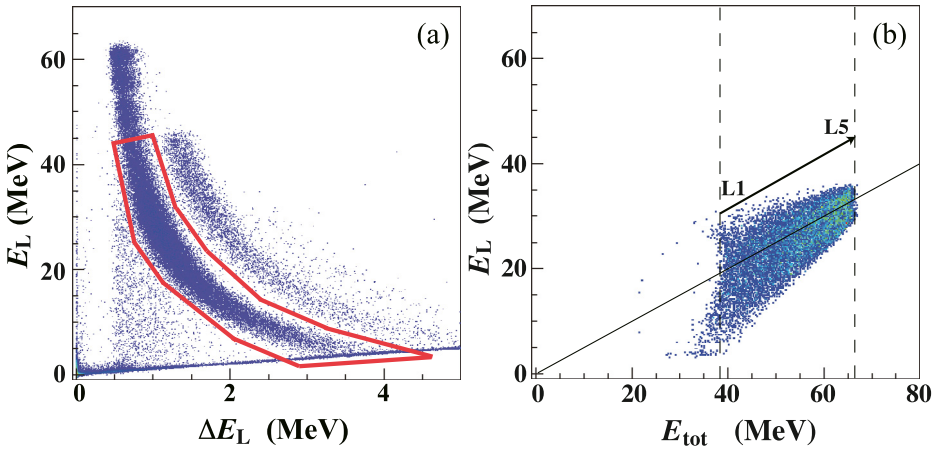

Fig. 5. (a) Scatter plot from the measurement with S^{4}AT at 75-kcps beam intensity showing the correlations between the measured E_L and ΔE_L with the left Si-CsI(Tl) telescope. The red polygon indicates the typical gate used to select elastically-scattered protons. (b) The total energy loss measured by the left (E_L) and the summed energy loss in the left and right telescopes (E_{tot}) after applying the proton gates from the left and right telescopes. The black arrow in (b) indicates roughly the depth position of the reaction vertex in the beam direction (L1–L5). The vertical dashed lines in the figure indicate the positions of z=0 and 5 mm, and are only a guide for the eye. The inclined solid line is the equal-energy line which represents the elastically-scattered protons with the same scattering angle.

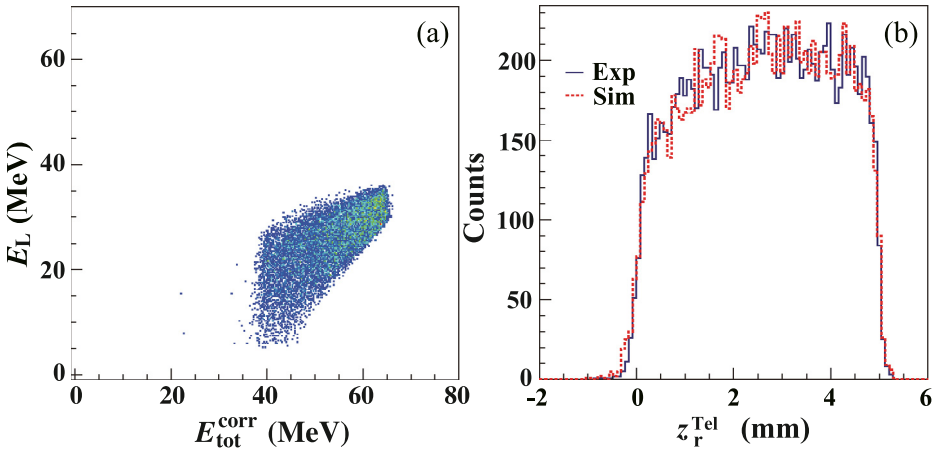

Fig. 6. (a) Total energy loss in the left telescope (E_L) against the corrected summed energy loss (E_{tot}^{corr}) for the measurement with S^{4}AT at 75-kcps beam intensity. (b) Reaction vertex distribution reconstructed from the total proton energies measured with the left and right SSD-CsI(Tl) telescopes. Only pp-elastic protons have been selected. The red-dotted histogram shows the results of the Monte Carlo simulation.

on their scattering angles (θ_L and θ_R). p_L and p_R penetrated the S^{4}AT detector, losing part of their energies before being stopped and detected by the SSD-CsI(Tl) telescopes. For simplicity, the kinetic energies of the protons measured by the left and right telescopes are denoted by E_L and E_R, respectively. In principle, $E_L + E_R$ ($\equiv E_{tot}$) should have a one-to-one correspondence with the reaction depth. However, as can be seen in Fig. 5(b), the E_{tot} distribution is skewed especially for protons with larger scattering angles (smaller E_L) due to their larger energy spread. This skewing effect was estimated using Monte Carlo simulations, and E_{tot} was corrected for each E_L value. The corrected distribution (E_{tot}^{corr}) is shown in Fig. 6(a). In this way, we obtained a linear conversion function between the total energy of the scattered protons and the reaction depth. The reconstructed depth distribution is shown in Fig. 6(b). For comparison, the depth distribution reconstructed from Monte Carlo simulation data is also shown (the red-dotted histogram). Overall, the simulation reproduced the experimental data very well.

It is important to note that the resolution of the reaction depth determined with the telescopes remained almost the same up to 3.6-Mcps proton beam, as shown in Fig. 7. The reaction events detected in L1, which include the events at $z < 0$ mm, are about 16% less compared to other layers, due to reduced telescope acceptance and shielding by the S^{4}AT supports for protons with large scattering angles. These missing events correspond to about 2% of the expected total pp-elastic events assuming that the elastic scattering cross section remains constant in all layers.

4.2. Vertex determination with S^{4}AT: Total energy-loss method

The depth of the reaction vertex can be determined by simply considering cumulative (total) energy loss of charged particles in S^{4}AT. This is equivalent to replacing the five layers by a single 5-mm-thick plastic scintillator. In this method, the total energy loss of the proton beam before reaction and the two protons (p_L and p_R) after reaction in S^{4}AT is measured. The total energy loss in S^{4}AT decreases with increasing z_r because p_L and p_R, which have lower energies and therefore higher dE/dx, penetrate through thinner plastic scintillator material at higher z_r. Fig. 8(a) shows the correlation between total energy loss (denoted by Q_{ATsum}) and the reaction depth determined using the SSD-CsI(Tl) telescopes as described in Section 4.1. Here, only events within the 'pp-elastic gates' have been selected. Events due to pile-up, which manifest in the form of energy-loss shifts as shown by the arrows, in S^{4}AT are clearly observed. The energy resolution for 1-MeV energy loss of a proton beam in a layer of S^{4}AT was about 18% at 75-kcps beam intensity. As will be discussed in Section 4.4, the reaction depth resolution depends on the energy resolution of S^{4}AT.

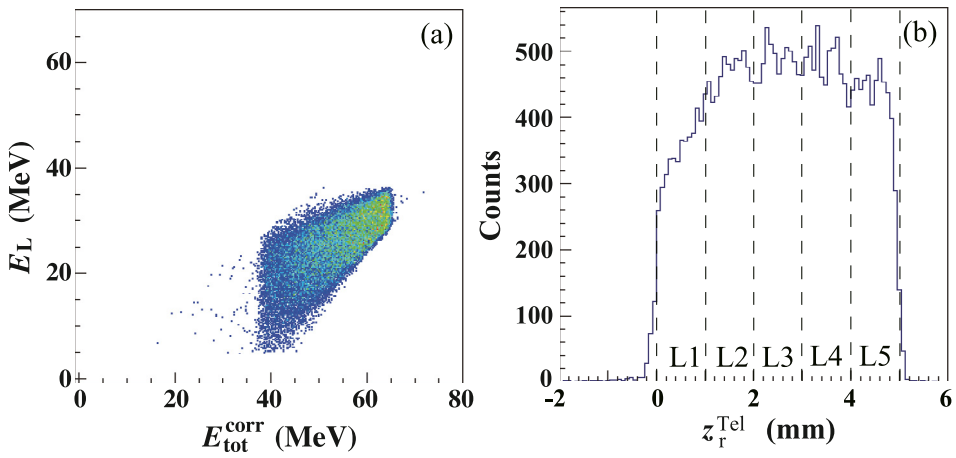

Fig. 7. (a) Total energy loss in the left telescope (E_L) against the corrected summed energy loss (E_{tot}^{corr}), and (b) reconstructed depth distribution for the measurement with 3.6-Mcps proton beam.

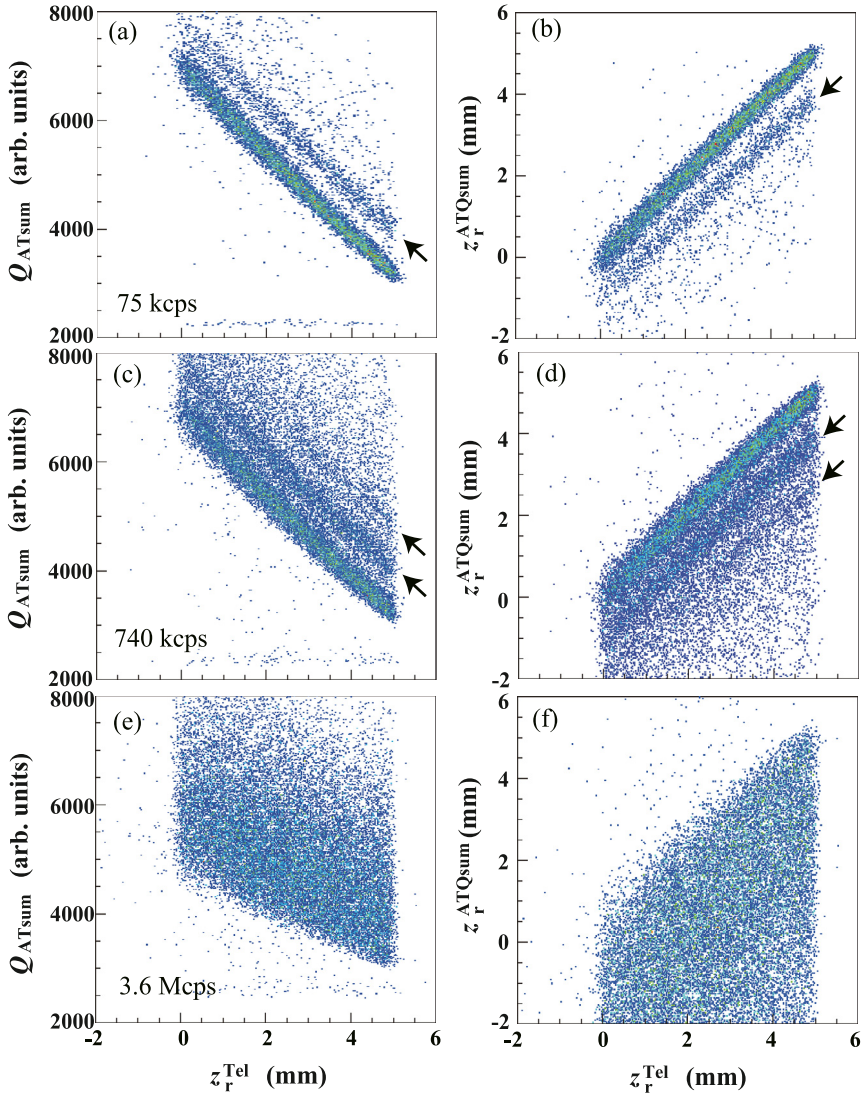

Fig. 8. (a)(c)(e) Total energy loss in S^4AT versus the reaction depth determined using the SSD-CsI(Tl) telescopes z_r^{Tel}, and (b)(d)(f) reaction depth reconstructed from the total energy loss in S^4AT, z_r^{ATQsum} versus z_r^{Tel}. (a) and (b), (c) and (d), (e) and (f) are for measurements with 75-kcps, 740-kcps and 3.6-Mcps beams, respectively. The arrows in (a)–(d) indicate shifts due to pile-ups.

To reconstruct the reaction depth from Q_{ATsum}, we derived a conversion formula using the single-hit events in Fig. 8(a). The resulting reaction depth (denoted by z_r^{ATQsum}) is plotted against z_r determined by the telescopes (denoted by z_r^{Tel}) in Fig. 8(b). For comparison, similar

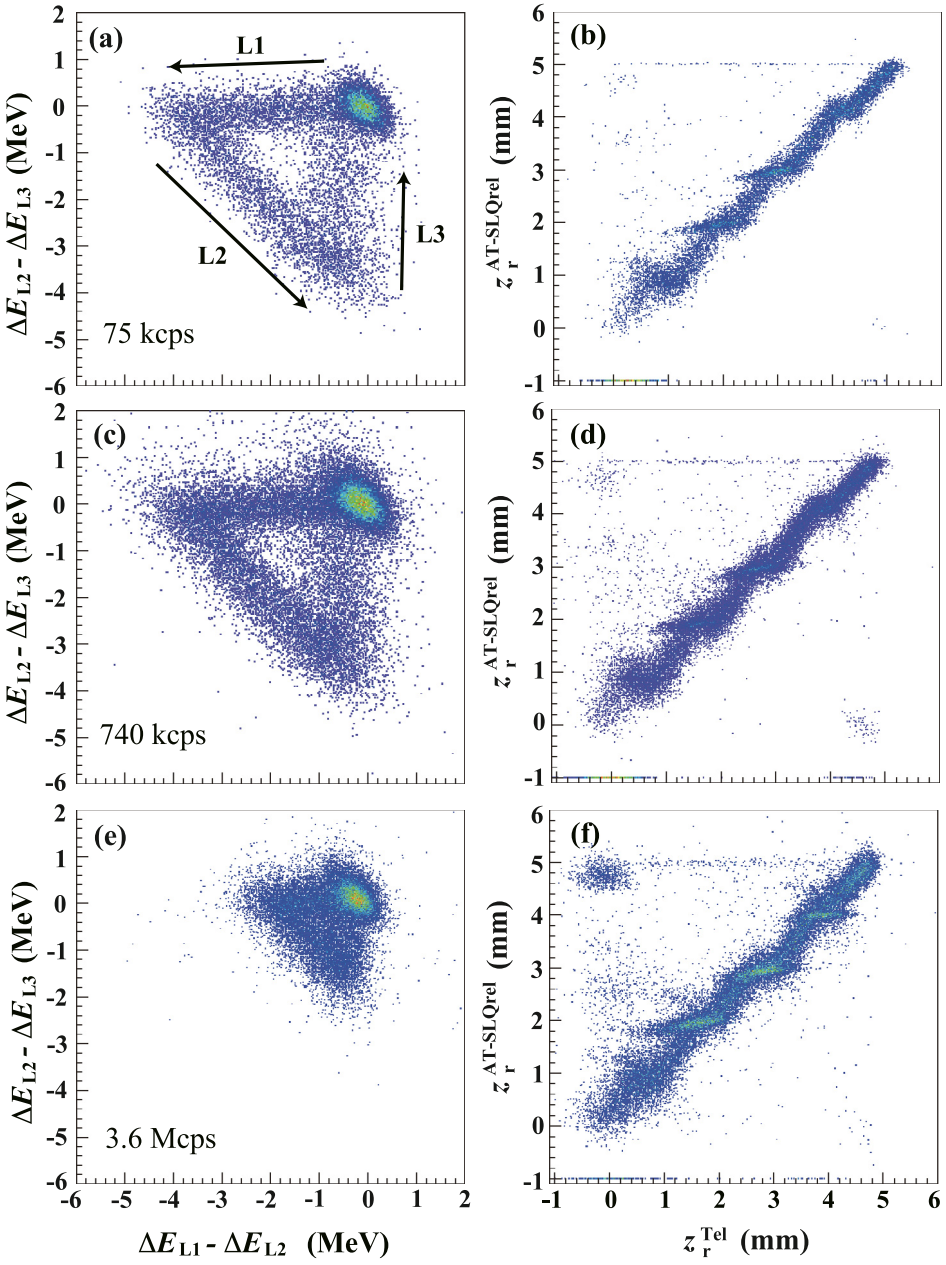

Fig. 9. (a) Energy-loss difference between L2 and L3 ($\Delta E_{L3} - \Delta E_{L2}$) versus energy-loss difference between L1 and L2 ($\Delta E_{L2} - \Delta E_{L1}$). The arrows indicate the direction of the depth position from L1 to L3. (b) Reaction depth, $z_r^{AT-SLQrel}$, reconstructed from single-layer energy-loss-difference method versus z_r^{Tel}. (c)–(d) and (e)–(f) are similar plots for the measurements with 740-kcps and 3.6-Mcps beams, respectively.

plots for the measurement with 740-kcps proton beam are shown in Fig. 8(c) and (d). The energy resolution deteriorates due to the increased pile-up events. It is important to note that although the single-hit, double-hit and even the triple-hit loci are still distinguishable, without the depth information from the telescope, it will be difficult to efficiently determine the reaction depth. The condition worsened at 3.6-Mcps beam intensity as shown in Fig. 8(e) and (f). Besides the deterioration in the energy and reaction depth resolutions, one observes, by comparing Fig. 8(e) with those of (c) and (a), clear reduction in the pulse heights of all anode signals. Such reduction is due to possible increased electron current which results in a drop in the interstage voltages for the dynodes in the MAPMTs, and consequently reduced collection efficiency and secondary electron emission. Although the gain-quenching effect can be addressed by modifying the last few stages of the MAPMTs to allow additional power supply boosters, the pile-up events will represent the major challenge for this method at a high-counting rate. In the next section, we demonstrate a novel method to address this issue.

4.3. Vertex determination with S^4AT: Energy-loss difference method

As mentioned earlier, the presence of nonreacted beam particle(s) in a reaction event results in a shift in the measured energy loss. For an intermediate-energy beam passing through thin layers of plastic scintillators, the energy loss of a beam particle in each layer is almost constant. Hence, this energy-loss shift, i.e. the effect of pile-up, can be eliminated by taking the energy-loss difference between adjacent layers. The simplest method is to consider energy loss in every single layer. Fig. 9(a) shows the scatter plot for the energy-loss difference between L2 and L3 ($\Delta E_{L3} - \Delta E_{L2}$) against the energy-loss difference between L1 and L2 ($\Delta E_{L2} - \Delta E_{L1}$) for the measurement with 75-kcps proton beam. Here, we have selected only coincident protons using

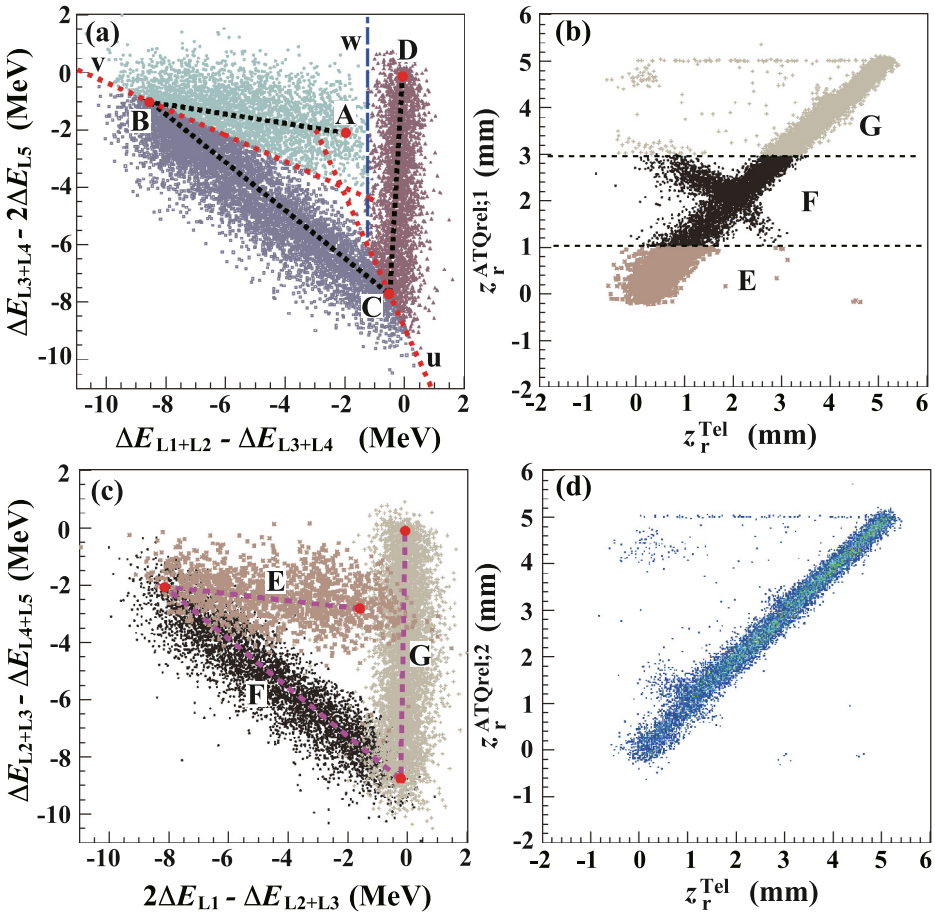

Fig. 10. (a) Correlation between $\Delta E_{L1+L2} - \Delta E_{L3+L4}$ and $\Delta E_{L3+L4} - 2\Delta E_{L5}$. (b) Reaction depth, denoted as $z_r^{ATQrel;1}$, reconstructed from the multi-layer energy-loss-difference correlation shown in (a) versus z_r^{Tel}. (c) Correlation between $\Delta E_{L2+L3} - \Delta E_{L4+L5}$ and $\Delta E_{L4+L5} - 2\Delta E_{L1}$. The colored events correspond to the events in the three regions separated by the two lines shown in (b). (d) Reaction depth, denoted as $z_r^{ATQrel;2}$, reconstructed from the multi-layer energy-loss-difference correlation shown in (c) versus z_r^{Tel}. The data are from measurements with 75-kcps proton beam.

the telescopes. Different points on the sides of the triangular locus correspond to different reaction depth in layers L1–L3. The arrows indicate the direction of the depth position. The dense elliptical events correspond to events reacted in L4 and L5. Similar correlations can be obtained by considering other combinations of energy-loss difference, and used to determine the reaction depth. This single-layer energy-loss-difference method, however, is subject to inherent uncertainties around the borders of adjacent layers, which correspond to the corners of the triangular locus in Fig. 9(a). For comparison, we plot the reaction depth reconstructed from this method, denoted as $z_r^{AT-SLQrel}$ against z_r^{Tel} in Fig. 9(b). Fig. 9(c) and (d) show similar plots as (a) and (b) but for the measurement with the 740-kcps beam. The loci in Fig. 9(c) are almost identical to those in Fig. 9(a), although the resolution looks slightly worse. Similar plots for the measurement with the 3.6-Mcps beam are shown in Fig. 9(e) and (f). Although the energy-loss differences shrink due to gain shift of the MAPMTs, it is still possible to determine the reaction depth by applying a universal scaling since the gain shift is common for all anodes. However, the uncertainties around the borders of adjacent layers and consequently, the depth resolutions deteriorate due to the worsening energy resolutions of the scintillators.

As a counter measure, we consider the correlation between $(\Delta E_{L1} + \Delta E_{L2}) - (\Delta E_{L3} + \Delta E_{L4})$ and $(\Delta E_{L3} + \Delta E_{L4}) - (2\Delta E_{L5})$. For simplicity, we rewrite $\Delta E_{L1} + \Delta E_{L2} = \Delta E_{L1+L2}$ and $\Delta E_{L3} + \Delta E_{L4} = \Delta E_{L3+L4}$. As an example, we show the correlation for the measurement with 75-kcps proton beam in Fig. 10(a). Notice that the L1–L2 (or L3–L4) border now lies on the straight locus AB (BC), which forms one of the sides of the open triangle. Besides addressing the border issue, summing the energy losses in two layers also helps to improve the energy resolution. This method, called the multi-layer energy-loss-difference method, consists of two stages of procedures. In the first stage, we used the correlation in Fig. 10(a) to determine the reaction depth. The procedures in the first stage are described as follows:

1. Determine central lines of the loci along L1–L2, L3–L4 and L5, as shown by the dashed lines in Fig. 10(a).
2. Determine the interior bisectors, lines denoted by "u" and "v", of the angles formed by ABC and BCD, as well as line "w"; the line "w" is parallel to the vertical axis, and corresponds to the minimum position of the projected $\Delta E_{L1+L2} - \Delta E_{L3+L4}$ distribution.
3. Divide the scatter plot into three straight loci using combinations of lines.
4. For each straight locus, determine a linear conversion formula for the reaction depth.

The reconstructed reaction depth, denoted as $z_r^{ATQrel;1}$, is plotted against z_r^{Tel} in Fig. 10(b). As shown in the figure, the uncertainties in the reconstructed reaction depth are relatively large near the borders of L2–L3 and L4–L5.

To reduce the uncertainties around the borders and improve the reaction depth determination, we consider, in the second stage, the correlation between $(\Delta E_{L3} + \Delta E_{L2}) - (\Delta E_{L5} + \Delta E_{L4})$ and $(2\Delta E_{L1}) - (\Delta E_{L5} + \Delta E_{L4})$, as shown in Fig. 10(c). By dividing $z_r^{ATQrel;1}$ into three regions, as indicated by E, F and G in Fig. 10(b), and selecting each region, three straight loci corresponding to the reaction depth in L1, L2–L3 and L4–L5 can be obtained. These straight loci were then used to determine

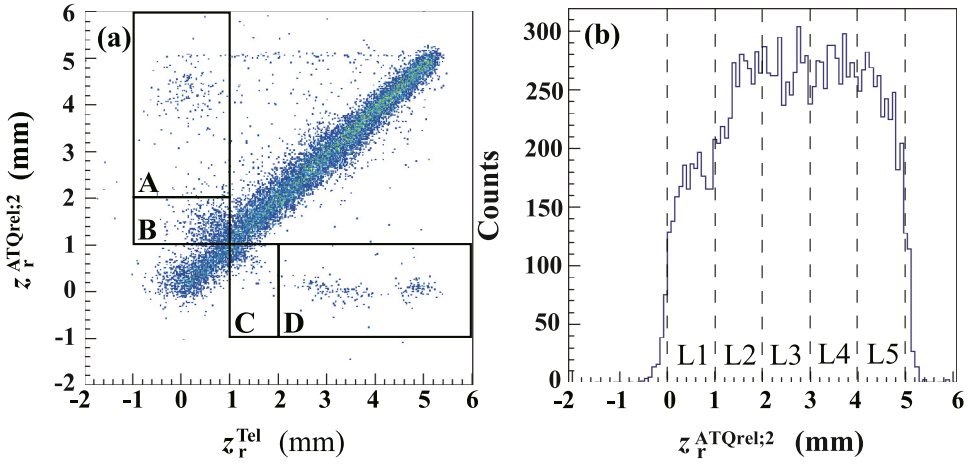

Fig. 11. (a) Reaction depth $z_r^{ATQrel;2}$ versus z_r^{Tel}, and (b) $z_r^{ATQrel;2}$ distribution for the measurement with 1.6-Mcps proton beam.

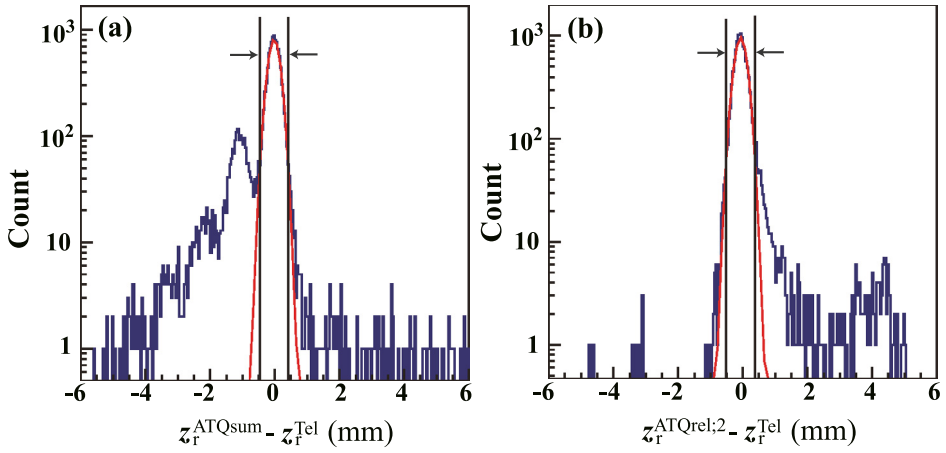

Fig. 12. $\Delta z^{AT} \equiv z_r^{AT} - z_r^{Tel}$ distributions for (a) $z_r^{AT} = z_r^{ATQsum}$ and (b) $z_r^{AT} = z_r^{ATQrel;2}$ for the measurements with 1.6-Mcps proton beam. The solid-vertical lines with arrows indicate the ranges for $|\Delta z^{AT}| \leq 2.33\sigma_z^{AT}$, where σ_z^{AT} is the root-mean-square width of the Δz^{AT} distribution around 0.

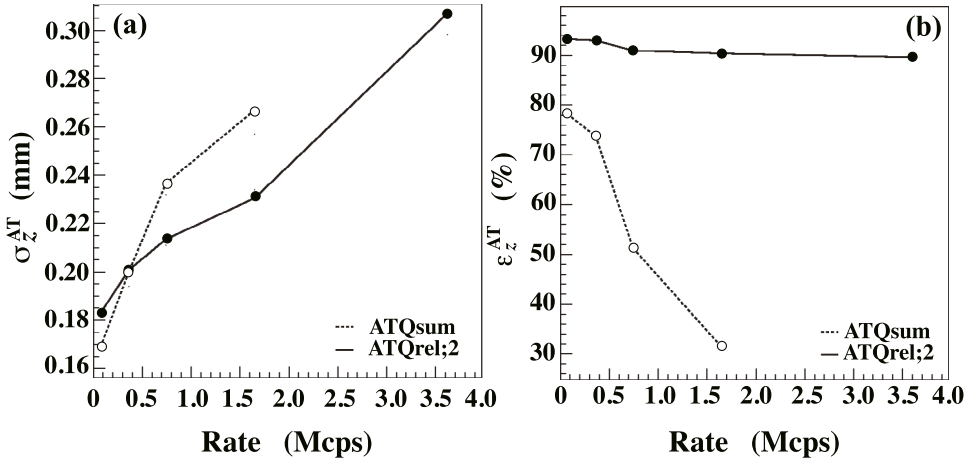

Fig. 13. Beam-intensity dependence of (a) reaction depth resolution, and (b) tracking efficiency.

the reaction depth, $z_r^{ATQrel;2}$. The reaction depth thus obtained is plotted against z_r^{Tel} in Fig. 10(d).

We applied this method to measurements with various beam intensities. Fig. 11 shows (a) the correlation between the reconstructed reaction depths using S^{4}AT ($z_r^{ATQrel;2}$) and the telescopes (z_r^{Tel}), and (b) the projected $z_r^{ATQrel;2}$ distribution for the measurement with 1.6-Mcps proton beam. The dashed lines in Fig. 11(b) have been added for reference. The reacted events in L1, which include also the events below 0 mm in Fig. 11(b), are about 28% less than in other layers. As mentioned in Section 4.1, 16% of the pp-elastic protons from L1 failed to reach the telescopes. The other 12% missing events are fairly accounted for by mis-reconstructions of reaction depth as shown by the four components in Fig. 11(a): missing A (−6%) and B (−20%) components, and additional C (+9%) and D (+6%) components. These

mis-reconstructions are due to the unresolved events in L1 and L5 around the vertical "w" line in Fig. 10(a) (components A and D), and in L1 and L2 around the intersection of the lines E and F in Fig. 10(c) (components B and C). Such unresolved events can be reduced by improving the energy resolution of the S^{4}AT system.

4.4. Resolution and tracking efficiency

The performance of S^{4}AT is evaluated in terms of the depth position resolution and tracking efficiency. To evaluate the depth position resolution, we consider the difference between the reaction depth determined using the telescopes and the one with S^{4}AT:

$$\Delta z^{\mathrm{AT}} \equiv z_{\mathrm{r}}^{\mathrm{AT}} - z_{\mathrm{r}}^{\mathrm{Tel}}, \tag{2}$$

where AT is "ATQsum" or "ATQrel;2". The Δz^{AT} distributions are shown in Fig. 12(a) and (b). The root-mean-square width of the Δz^{AT} distribution around 0, denoted as σ_z^{AT}, is taken as the effective depth position resolution, which is attributed to the intrinsic energy resolutions of the plastic scintillators and the telescopes. The tracking efficiency is defined as

$$\epsilon_z^{\mathrm{AT}} \equiv N(|\Delta z^{\mathrm{AT}}| \le 2.33\sigma_z^{\mathrm{AT}})/N(-1 < z_{\mathrm{r}}^{\mathrm{Tel}} < 6), \tag{3}$$

where $N(|\Delta z^{\mathrm{AT}}| \le 2.33\sigma_z^{\mathrm{AT}})$ represents the number of events with Δz^{AT} within $2.33\sigma_z^{\mathrm{AT}}$ or 98% confidence level, and $N(-1 < z_{\mathrm{r}}^{\mathrm{Tel}} < 6)$ the number of events successfully tracked by the telescopes. The dependences of σ_z^{AT} and ϵ_z^{AT} on the beam intensity are plotted in Fig. 13. The results show that $\sigma_z^{\mathrm{ATQsum}}$ ($\epsilon_z^{\mathrm{ATQsum}}$) increases (decreases) with increasing beam intensity. It is extremely difficult or even impossible to determine the reaction depth for beam intensities beyond 1.6 Mcps. This issue does not arise with the multi-layer energy-loss-difference method. Although $\sigma_z^{\mathrm{ATQrel;2}}$ worsens slightly, increasing from about 0.18 mm at 75 kcps to about 0.23 at 1.6 Mcps, we achieved a resolution of about 0.31 mm at 3.6 Mcps. The tracking efficiency $\epsilon_z^{\mathrm{ATQrel;2}}$ remains high at 90% even at 3.6 Mcps.

The actual depth resolution of S^{4}AT is expected to be better than the effective depth resolution $\sigma_z^{\mathrm{ATQrel;2}}$. As an example, we estimated the actual depth position resolutions for S^{4}AT and the Si-CsI(Tl) telescopes using Monte Carlo simulations taking into account the experimental conditions. For simplicity, we considered the case with a 75-kcps proton beam. Since the actual reaction depth position for each event is known in the simulation, one can calculate the deviations of the simulated reconstructed depth positions with S^{4}AT and the Si-CsI(Tl) telescopes from the actual reaction depth position. The depth position resolutions, defined as the root-mean-square widths of the deviation distributions, were estimated to be about 0.14 and 0.13 mm for S^{4}AT and the Si-CsI(Tl) telescopes, respectively. The combined resolution is 0.19 mm, which is almost equal to the experimental value (0.18 mm). Hence, the actual depth resolution achieved at 3.6-Mcps is expected to be below 0.31 mm (one sigma).

Finally, it is useful to understand the effect of the intrinsic energy resolution of the multi-layer plastic scintillators on the depth resolution of S^{4}AT. To investigate the dependence on the intrinsic energy resolution, we performed Monte Carlo simulations based on the present experimental setup. For simplicity, we assumed that all layers have the same intrinsic energy resolutions. By artificially changing the intrinsic energy resolution, we performed simulations to estimate the depth resolution $\sigma_z^{\mathrm{ATQrel;2}}$. The results are plotted in Fig. 14 as a function of energy resolution for 1-MeV energy loss of a proton in a layer of S^{4}AT, which is denoted by $\sigma_{\mathrm{ATQ;L}_i}$. As mentioned in Section 4.2, $\sigma_{\mathrm{ATQ;L}_i}$ was about 18% at 75-kcps beam intensity in the present work. This relatively poor intrinsic energy resolution was due to light leakage into neighboring anode strips, which resulted in a relatively low light collection efficiency (about 60%) in one anode strip. Further reduction in $\sigma_{\mathrm{ATQ;L}_i}$ is anticipated in future experiments by adding back the output signals from neighboring anodes.

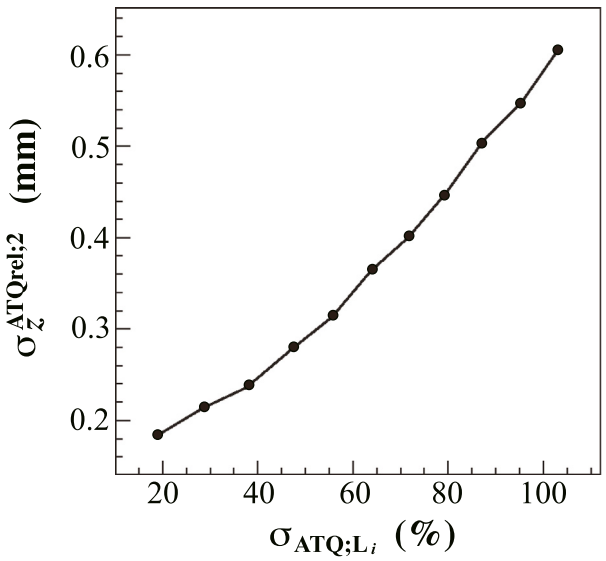

Fig. 14. Dependence of reaction depth resolution on intrinsic energy resolution of the plastic scintillators.

5. Summary and future prospects

We have constructed and tested a novel prototype solid-state active proton target, named Stack Structure Solid organic Scintillator Active Target (S^{4}AT), for use in nuclear spectroscopic studies with nuclear reactions in inverse kinematics. The solid active target consists of five layers of plastic scintillators, each with a 1-mm thickness. S^{4}AT offers the capability to determine the reaction depth through exploitation of the difference between the energy losses of a charged beam particle and charged reaction products in the scintillator material. By considering the relative energy loss between different layers, the energy loss due to unreacted beam particles can be eliminated. The ability to eliminate pile-up effects enables its operation at a moderate beam intensity of up to a few Mcps. To evaluate its performance, we have performed an elastic proton–proton measurement using a 70-MeV proton beam at Cyclotron and Radioisotope Center (CYRIC), Tohoku University. The depth resolution achieved was below 0.31 mm (one sigma) at 3.6-Mcps proton beam intensity.

One of the two remaining issues is the gain shift, which will be the most critical issue for operation at higher beam intensity. To address this issue, we plan to introduce additional power supply boosters to the last few stages of the MAPMT. The other issue is related to its performance with different types of beam. The present test experiment was performed using a proton beam from a cyclotron. It will be useful and important also to perform a test experiment using a beam from a synchrotron accelerator, because of the difference in the time structure of the beam, i.e. the pile-up frequency.

The present system offers the prospect of a relatively thick target while maintaining a good energy resolution. It is worth noting that by replacing the plastic scintillators with the deuterated ones such as the BC436 [22], one can also construct a solid-state active deuteron target system.

Declaration of competing interest

The authors declare that they have no known competing financial interests or personal relationships that could have appeared to influence the work reported in this paper.

CRediT authorship contribution statement

D.T. Tran: Formal analysis, Investigation, Methodology, Software, Visualization, Writing - review & editing. **S. Terashima:** Conceptualization, Data curation, Project administration, Supervision, Investigation, Methodology, Software, Visualization, Writing - review & editing. **H.J. Ong:** Conceptualization, Data curation, Project administration, Supervision, Funding acquisition, Investigation, Methodology, Software, Visualization, Resources, Writing - original draft, Writing - review & editing. **K. Hirakawa:** Formal analysis, Investigation. **Y. Matsuda:** Investigation, Resources. **N. Aoi:** Funding acquisition, Resources. **M.N. Harakeh:** Writing - review & editing. **M. Itoh:** Investigation, Resources. **T. Kawabata:** Resources. **A. Kohda:** Investigation. **S.Y. Matsumoto:** Investigation. **T. Nishi:** Investigation. **J. Okamoto:** Investigation. **I. Tanihata:** Funding acquisition, Resources.

Acknowledgments

The authors thank the CYRIC operators for the stable proton beam and the CYRIC administrative staff for support. We also acknowledge hardware support from T. Furuno and J. Zenihiro. This work was partially supported by Hirose International Scholarship Foundation, the National Natural Science Foundation of China under Contracts No. 11235002, No. 11375023, No. 11475014, and No. 11575018, and the National Key R & D program of China (2016YFA0400504).

References

[1] I. Tanihata, H. Hamagaki, O. Hashimoto, Y. Shida, N. Yoshikawa, K. Sugimoto, O. Yamakawa, T. Kobayashi, N. Takahashi, Measurements of interaction cross sections and nuclear radii in the light *p*-shell region, Phys. Rev. Lett. 55 (1985) 2676–2679, http://dx.doi.org/10.1103/PhysRevLett.55.2676.

[2] O. Sorlin, M.G. Porquet, Nuclear magic numbers: New features far from stability, Prog. Part. Nucl. Phys. 61 (2008) 602–673, http://dx.doi.org/10.1016/j.ppnp.2008.05.001.

[3] T. Nakamura, H. Sakurai, H. Watanabe, Exotic nuclei explored at in-flight separators, Prog. Part. Nucl. Phys. 97 (2017) 53–122, http://dx.doi.org/10.1016/j.ppnp.2017.05.001.

[4] D.T. Tran, H.J. Ong, G. Hagen, T.D. Morris, N. Aoi, T. Suzuki, Y. Kanada-En'yo, L.S. Geng, S. Terashima, I. Tanihata, T.T. Nguyen, Y. Ayyad, P.Y. Chan, M. Fukuda, H. Geissel, M.N. Harakeh, T. Hashimoto, T.H. Hoang, E. Ideguchi, A. Inoue, G.R. Jansen, R. Kanungo, T. Kawabata, L.H. Khiem, W.P. Lin, K. Matsuta, M. Mihara, S. Momota, D. Nagae, N.D. Nguyen, D. Nishimura, T. Otsuka, A. Ozawa, P.P. Ren, H. Sakaguchi, C. Scheidenberger, J. Tanaka, M. Takechi, R. Wada, T. Yamamoto, Evidence for prevalent Z=6 magic number in neutron-rich carbon isotopes, Nature Commun. 9 (2018) 1594, http://dx.doi.org/10.1038/s41467-018-04024-y.

[5] T. Otsuka, T. Suzuki, R. Fujimoto, H. Grawe, Y. Akaishi, Evolution of nuclear shells due to the tensor force, Phys. Rev. Lett. 95 (2005) 232502, http://dx.doi.org/10.1103/PhysRevLett.95.232502.

[6] T. Myo, K. Kato, H. Toki, K. Ikeda, Roles of tensor and pairing correlations on halo formation in ^{11}Li, Phys. Rev. C 76 (2007) 024305, http://dx.doi.org/10.1103/PhysRevC.76.024305.

[7] H.J. Ong, I. Tanihata, A. Tamii, T. Myo, K. Ogata, M. Fukuda, K. Hirota, K. Ikeda, D. Ishikawa, T. Kawabata, H. Matsubara, K. Matsuta, M. Mihara, T. Naito, D. Nishimura, Y. Ogawa, H. Okamura, A. Ozawa, D.Y. Pang, H. Sakaguchi, K. Sekiguchi, T. Suzuki, M. Taniguchi, M. Takashina, H. Toki, Y. Yasuda, M. Yosoi, J. Zenihiro, Probing effect of tensor interactions in ^{16}O via (p,d) reaction, Phys. Lett. B 725 (2013) 277–281, http://dx.doi.org/10.1016/j.physletb.2013.07.038.

[8] S. Terashima, L. Yu, H.J. Ong, I. Tanihata, S. Adachi, N. Aoi, P.Y. Chan, H. Fujioka, M. Fukuda, H. Geissel, G. Gey, J. Golak, E. Haettner, C. Iwamoto, T. Kawabata, H. Kamada, X.Y. Le, H. Sakaguchi, A. Sakaue, C. Scheidenberger, R. Skibiski, B.H. Sun, A. Tamii, T.L. Tang, D.T. Tran, K. Topolnicki, T.F. Wang, Y.N. Watanabe, H. Weick, H. Witaa, G.X. Zhang, L.H. Zhu, Dominance of tensor correlations in high-momentum nucleon pairs studied by (p,pd) reaction, Phys. Rev. Lett. 121 (2018) 242501, http://dx.doi.org/10.1103/PhysRevLett.121.242501.

[9] E. Pollacco, D. Beaumel, P. Roussel-Chomaz, E. Atkin, P. Baron, J.P. Baronick, E. Becheva, Y. Blumenfeld, A. Boujrad, A. Drouart, F. Druillole, P. Edelbruck, M. Gelin, A. Gillibert, C. Houarner, V. Lapoux, L. Lavergne, G. Leberthe, L. Leterrier, V.L. Ven, F. Lugiez, L. Nalpas, L. Olivier, B. Paul, B. Raine, A. Richard, M. Rouger, F. Saillant, F. Skaza, M. Tripon, M. Vilmay, E. Wanlin, M. Wittwer, MUST2: A new generation array for direct reaction studies, Eur. Phys. J. A 25 (2005) 287–288, http://dx.doi.org/10.1140/epjad/i2005-06-162-5.

[10] M.S. Wallacea, M.A. Famiano, M.J. van Goethem, A.M. Rogers, W.G. Lynch, J. Clifford, F. Delaunay, J. Lee, S. Labostov, M. Mocko, L. Morris, A. Moroni, B.E. Nett, D.J. Oostdyk, R. Krishnasamy, M.B. Tsang, R.T. de Souza, S. Hudan, L.G. Sobotka, R.J. Charity, J. Elson, G.L. Engel, The high resolution array (HiRA) for rare isotope beam experiments, Nucl. Instrum. Methods Phys. Res. A 583 (2007) 302–312, http://dx.doi.org/10.1016/j.nima.2007.08.248.

[11] T. Hashimoto, H. Ishiyama, T. Ishikawa, T. Kawamura, K. Nakai, Y.X. Watanabe, H. Miyatake, M.H. Tanaka, Y. Fuchi, N. Yoshikawa, S.C. Jeong, I. Katayama, T. Nomura, T. Furukawa, S. Mitsuoka, K. Nishio, M. Matsuda, H. Ikezoe, T. Fukuda, S.K. Das, P.K. Saha, Y. Mizoi, T. Komatsubara, M. Yamaguchi, Y. Tagishi, Gated multiple-sampling and tracking proportional chamber: New detector system for nuclear astrophysical study with radioactive nuclear beams, Nucl. Instrum. Methods Phys. Res. A 556 (2006) 339–349, http://dx.doi.org/10.1016/j.nima.2005.10.018.

[12] C.E. Demonchy, W. Mittig, H. Savajols, P. Roussel-Chomaz, M. Chartier, B. Jurado, L. Giot, D. Cortina-Gil, M. Caamaño, G. Ter-Arkopian, A. Fomichev, A. Rodin, M.S. Golovkov, S. Stepantsov, A. Gillibert, E. Pollacco, A. Obertelli, H. Wang, MAYA, a gaseous active target, Nucl. Instrum. Methods Phys. Res. A 573 (2007) 145–148, http://dx.doi.org/10.1016/j.nima.2006.11.025.

[13] D. Suzuki, M. Ford, D. Bazin, W. Mittig, W.G. Lynch, T. Ahn, S. Aune, E. Galyaev, A. Fritsch, J. Gilbert, F. Montes, A. Shore, J. Yurkon, J.J. Kolata, J. Browne, A. Howard, A.L. Roberts, X.D. Tang, Prototype AT-TPC:toward a new generation active target time projection chamber for radioactive beam experiments, Nucl. Instrum. Methods Phys. Res. A 691 (2012) 39–54, http://dx.doi.org/10.1016/j.nima.2012.06.050.

[14] S. Ota, H. Tokieda, C.S. Lee, Y.N. Watanabe, CNS active target (CAT) for missing mass spectroscopy with intense beams, J. Radioanal. Nucl. Chem. 305 (2015) 907–911, http://dx.doi.org/10.1007/s10967-015-4130-5.

[15] T. Furuno, T. Kawabata, H.J. Ong, S. Adachi, Y. Ayyad, T. Baba, Y. Fujikawa, T. Hashimoto, K. Inaba, Y. Ishii, S. Kabuki, H. Kubo, Y. Matsuda, Y. Matsuoka, T. Mizumoto, T. Morimoto, M. Murata, T. Sawano, T. Suzuki, A. Takada, J. Tanaka, I. Tanihata, T. Tanimori, D.T. Tran, M. Tsumura, H.D. Watanabe, Performance test of the MAIKo active target, Nucl. Instrum. Methods Phys. Res. A 908 (2018) 215–224, http://dx.doi.org/10.1016/j.nima.2018.08.042.

[16] L. Yu, S. Terashima, H.J. Ong, P.Y. Chan, I. Tanihata, C. Iwamoto, D.T. Tran, A. Tamii, N. Aoi, H. Fujioka, G. Gey, H. Sakaguchi, A. Sakaue, B.H. Sun, T.L. Tang, T.F. Wang, Y.N. Watanabe, G.X. Zhang, Multi-layer plastic scintillation detector for intermediate- and high-energy neutrons with n-γ discrimination capability, Nucl. Instrum. Methods Phys. Res. A 866 (2017) 118–128, http://dx.doi.org/10.1016/j.nima.2017.05.044.

[17] W. Horiuchi, Y. Suzuki, Momentum distribution and correlation of two-nucleon relative motion in ^{6}He and ^{6}Li, Phys. Rev. C 76 (2007) 024311, http://dx.doi.org/10.1103/PhysRevC.76.024311.

[18] H. Baba, T. Ichihara, T. Ohnishi, S. Takeuchi, K. Yoshida, Y. Watanabe, S. Ota, S. Shimoura, New data acquisition system for the RIKEN radioactive isotope beam factory, Nucl. Instrum. Methods Phys. Res. A 616 (2010) 65–68, http://dx.doi.org/10.1016/j.nima.2010.02.120.

[19] R. Brun, F. Rademakers, ROOT – an object oriented data analysis framework, Nucl. Instrum. Methods Phys. Res. A 389 (1997) 81–86, http://dx.doi.org/10.1016/S0168-9002(97)00048-X.

[20] S. Agostinelli, J. Allison, et al., GEANT4 – a simulation toolkit, Nucl. Instrum. Methods Phys. Res. A 506 (2003) 250–303, http://dx.doi.org/10.1016/S0168-9002(03)01368-8.

[21] R.M. Brown, D.J.A. Cockerill, Electromagnetic calorimetry, Nucl. Instrum. Methods Phys. Res. A 666 (2012) 47–79, http://dx.doi.org/10.1016/j.nima.2011.03.017.

[22] J. Frenje, S. Conroy, G. Ericsson, J. Källne, P.-U. Renberg, E. Traneus, Deuterated plastic scintillator for proton detection in a neutron background, Nucl. Instrum. Methods Phys. Res. A 376 (1996) 462–465, http://dx.doi.org/10.1016/0168-9002(96)00162-3.